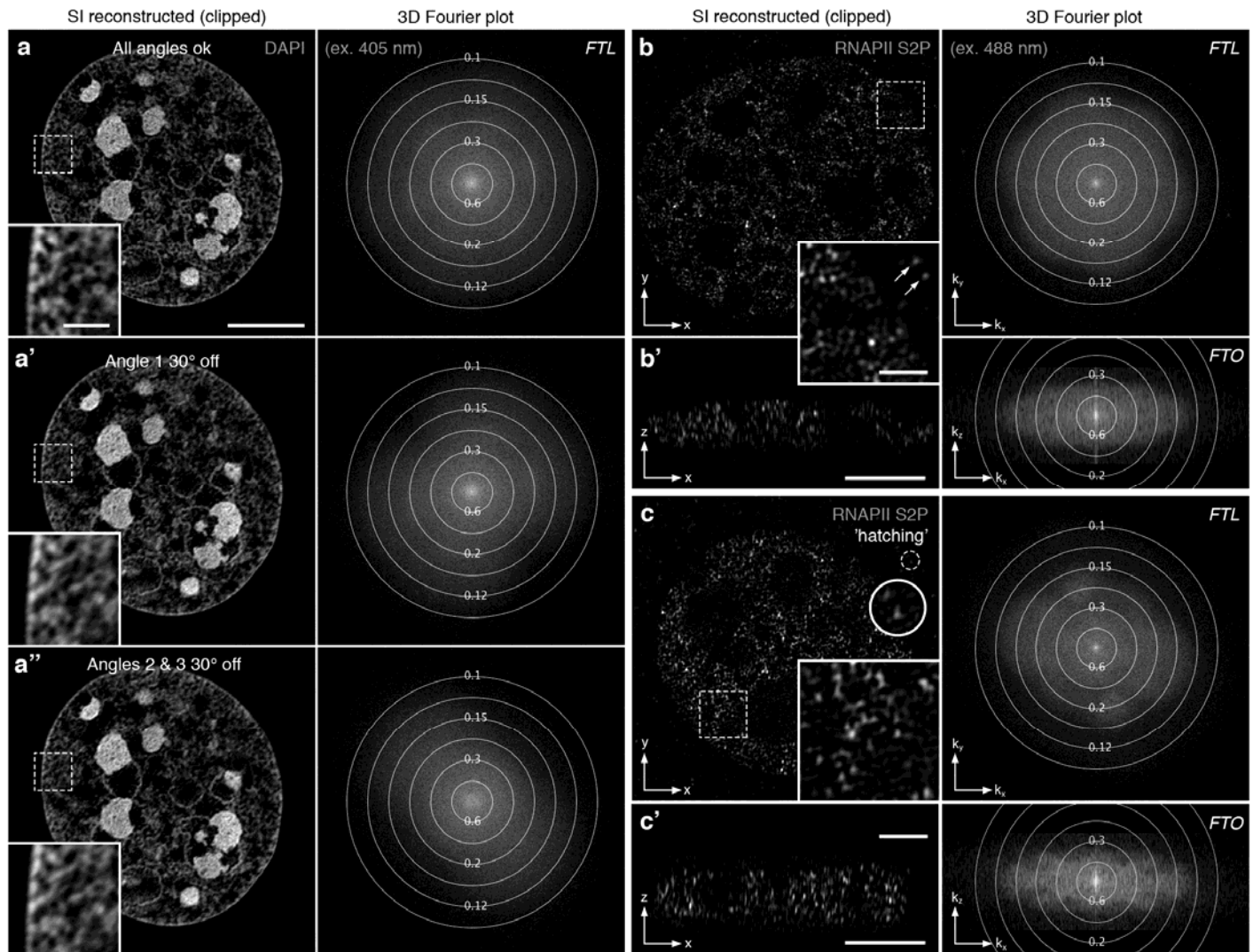


Supplementary Figure 1

Reconstructed noise artifact as a function of modulation contrast in the SIM raw data

Datasets progress from having a very low signal-to-noise ratio (SNR) (far left column) up to an acceptable SNR (far right column) with initial acquisition conditions directly affecting quality of the resulting reconstruction. Data collected from wild type C127 mouse cells immunostained for tubulin (Alexa Fluor 488) are presented as: representative frames of raw datasets, with stripes shown in one angular direction (top row); modulation contrast to noise ratio (MCNR) in the raw data mapped onto the reconstructed dataset (MCN readout of SIMcheck; maximum projections; second row); reconstructed single-slice images showing the full dynamic range (third row); reconstructed single-slice images showing the dynamic range after cut-off below the mode value of the intensity histogram (fourth row). Reconstruction intensity histograms (fifth row) of reconstructed 32-bit data are shown as log-scaled (grey) or linear-scaled (black) intensity values, with the x-axis representing pixel intensity in the given range. The values removed in the mode-based cut-off overlaid in red, and the ratio between minimum and maximum values in the histogram (MMR) is expressed above each plot. Lateral 3D Fourier plots (*FTL*, sixth row) of the reconstructed data are shown with reciprocal distance in μm plotted as circles over the FFT. The radial profiles (*FTR*, last row) display the corresponding radially averaged amplitudes with the red line indicating a reference amplitude value (22, arbitrary units) for comparison. Note that with increasing signal-to-noise the profiles become smoother and the area between the reference and the curve become larger. For each image, the dashed box indicates the inset region. Scale bars: 5 μm and 1 μm (inset). For each row, T indicates % transmission of the 488 nm laser, and exp. indicates the exposure time. Images were acquired on a GE OMX V3 Blaze instrument equipped with an Olympus 60x/1.42 PlanApo N objective and PCO edge 4.2 sCMOS cameras.

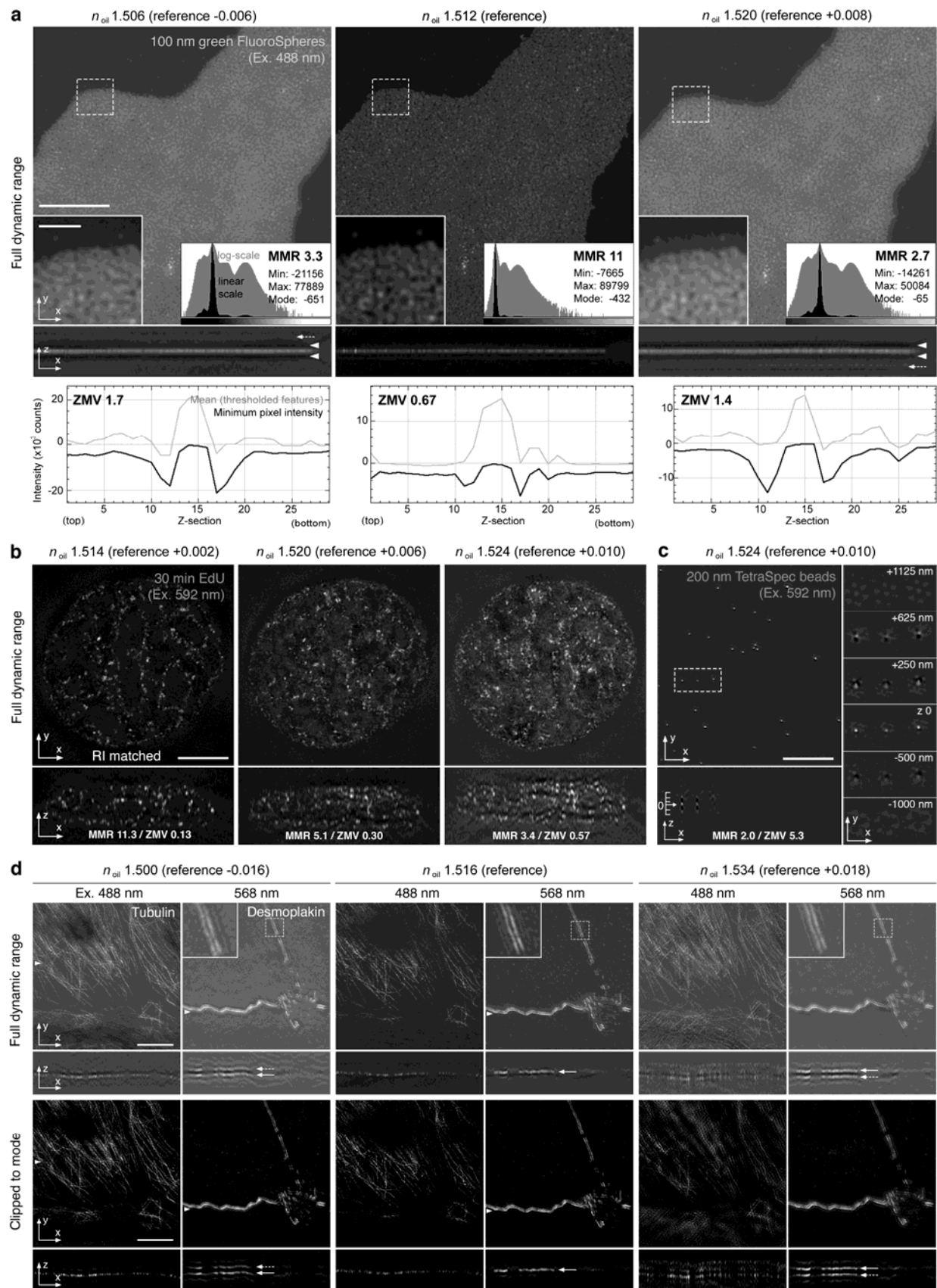


Supplementary Figure 2

Illustration of 'hatching' artifacts caused by missing angle information

Data collected from wild type C127 mouse cells stained with either (a) DAPI to label chromatin distribution or (b, c) immunostained for RNA polymerase II phosphorylated at serine 2 of the C-terminal domain (RNAPII S2P). These showcase the effect of missing angular frequency information on complex (chromatin) or punctate (RNAPII) labeled features, supplementary to **Fig. 1c**. (a-a'') Reconstruction of the same dataset with correct angle (k_0) settings (a), and with a false k_0 parameter settings for either one (a') or two (a'') angles, respectively. Note that the loss of lateral resolution enhancement is particularly evident in the corresponding Fourier plots with frequency extensions missing for the affected angles (second column). Accordingly, the labeled features in the reconstructed images (insets) are less sharp. (b, c) Reconstruction of punctate nuclear RNAPII signals with correctly fitted k_0 value (b) compared to a dataset where the k_0 fitting failed for two of the three angle directions (c). Detailed view of the reconstructed lateral midsection highlight elongated features of nuclear signals in c, but not in b (boxed insets). Single cytoplasmic background signals (originating from unspecific bound antibody complexes) show 'starfish' extensions in the faulty dataset (circular inset in c) while similar signals are round in the well-reconstructed dataset (arrows, inset in b). While not easily noticeable in the reconstructed image, the absence or presence of hatching becomes apparent in the corresponding Fourier

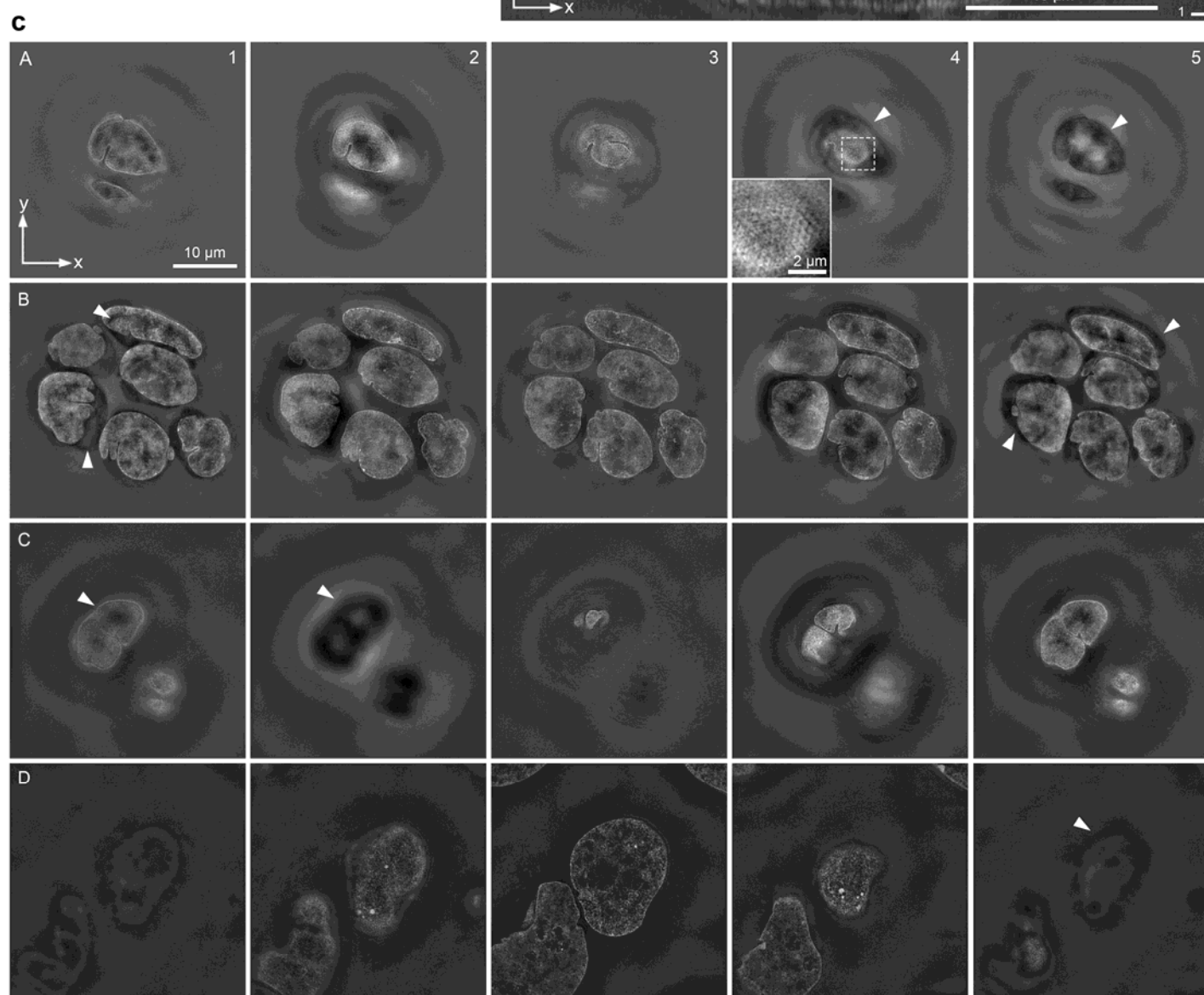
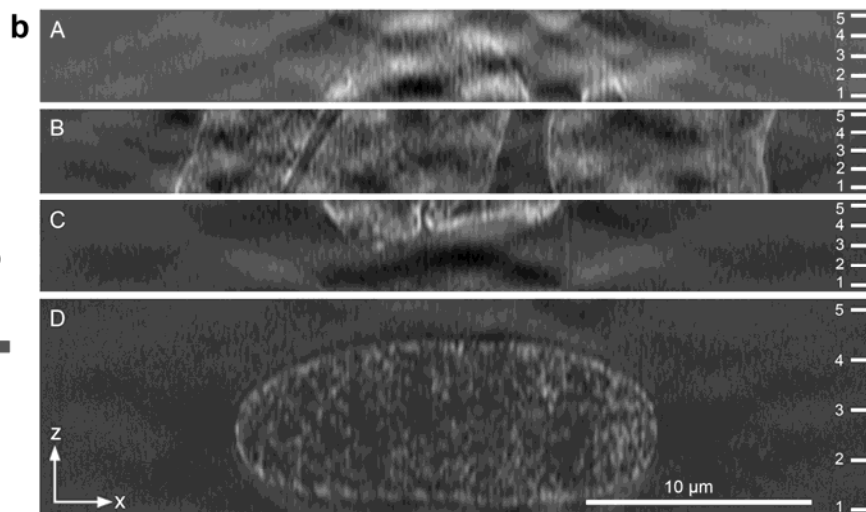
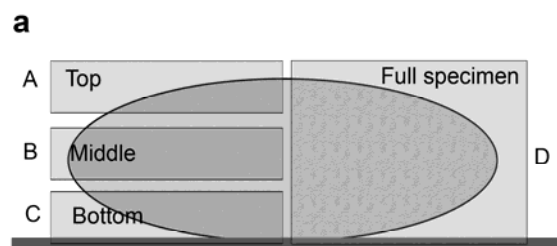
plot. Of note, enhancement of the axial resolution, as well as contrast increase by out-of-focus signal suppression are hardly affected, as highlighted by the comparison of the the orthogonal sections and the corresponding orthogonal Fourier plots in **b'** and **c'**. Scale bars: 5 μm and 1 μm (insets). Images were acquired on a GE OMX V3 Blaze instrument equipped with an Olympus 60x/1.42 PlanApo N objective and PCO edge 4.2 sCMOS cameras.



Supplementary Figure 3

Illustration of refractive index mismatch induced artifacts

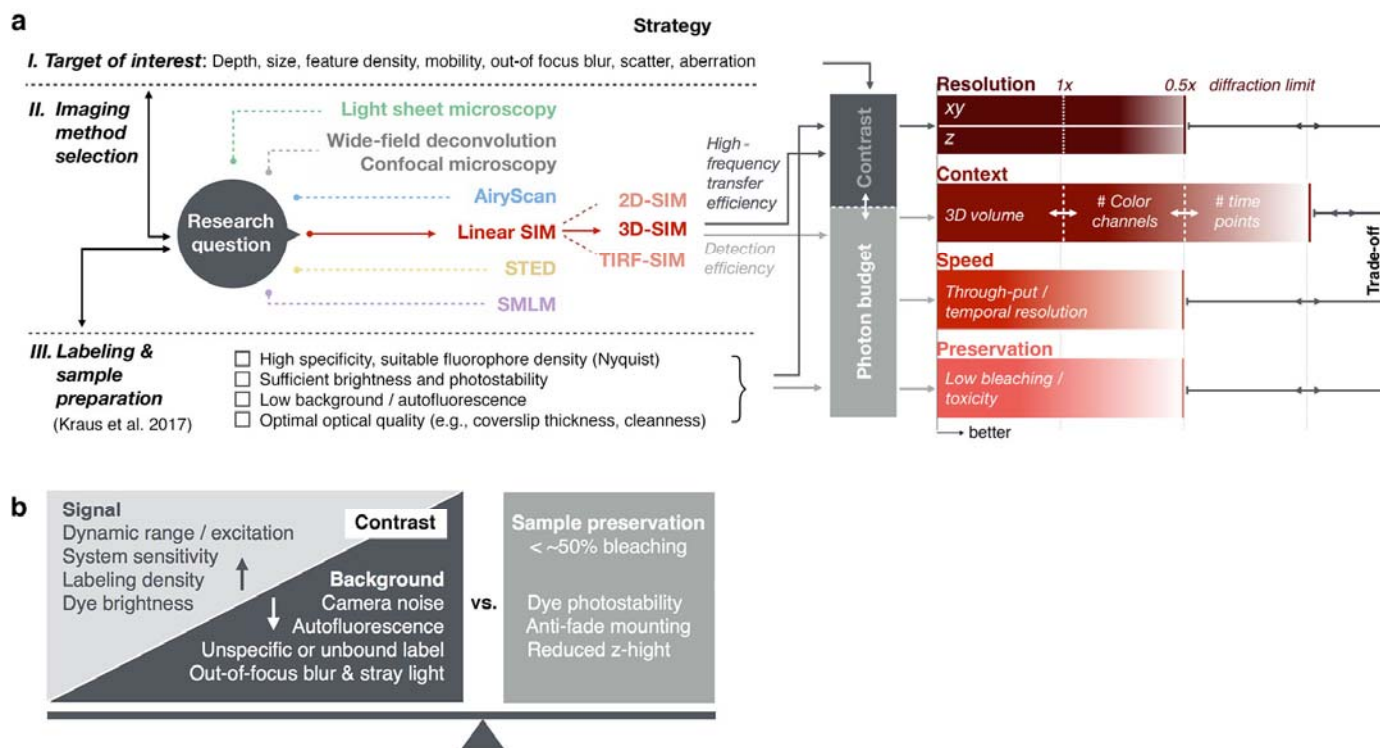
(a) Mounting medium refractive index (RI) matched to the sample will exaggerate or suppress the z-ghosting artifact, as observed in lateral and orthogonal views of sub-diffraction sized FluoSphere green (Ex. 488 λ) coverslip beads (*Ref.* calibration slide #1). As the acquisition medium's refractive index (RI) is varied from too low (left) to optimally matched (middle) to too high (right) reconstruction of the depicted area is seen to increase in quality nearest the sample's reference oil. Orthogonal views highlight that an extreme mismatch (>5 units change from reference RI) produces images with prominent intensity dips (arrowheads) in z-slices adjacent to sample real signal. Additionally, undershooting the sample's RI-match can result in a noticeable ghost image in z-slices atop real signal while overshooting this match results in a ghost image of beads repeated in z-slices beneath real signal (dotted arrows). (b) Effect of increasing RI mismatch on a punctate nuclear staining pattern (EdU pulse replication labeling and detection with click chemistry in C127 cells). Note the intermixing of real and ghost signals in the orthogonal views with increasing mismatch. (c) RI mismatch on very bright isolated features (here 200 nm diameter TetraSpeck beads) produces characteristic hexagonal patterns of the out-of-focus echo signal, highlighted in the detailed view of individual z-planes through a selected bead (right). (d) Image series supplementary to **Fig. 1e** demonstrating ghosting on an MDCK cell immunostained for tubulin (Alexa Fluor 488) and desmoplakin C-terminus (Alexa Fluor 568) to emphasize the ease in diagnosing intensity dips from an RI-mismatch in images prior to any thresholding. Upper row of panels shows the lateral (top panel) and orthogonal (bottom panel) cross section of the reconstructed dataset with the full dynamic range, while the lower row shows the same data after intensity cut-off at zero. Arrowhead (first column) indicates position of the orthogonal view. Scale bar: 5 μ m. Images in (a-c) were acquired on a GE OMX V3 Blaze instrument with PCO edge 4.2 sCMOS cameras; images in (d) were acquired on a GE OMX V4 Blaze instrument equipped with an Olympus 100x/1.40 SApo objective and Photometrics Evolve EMCCD cameras.



Supplementary Figure 4

Illustration of z-wrapping artifacts

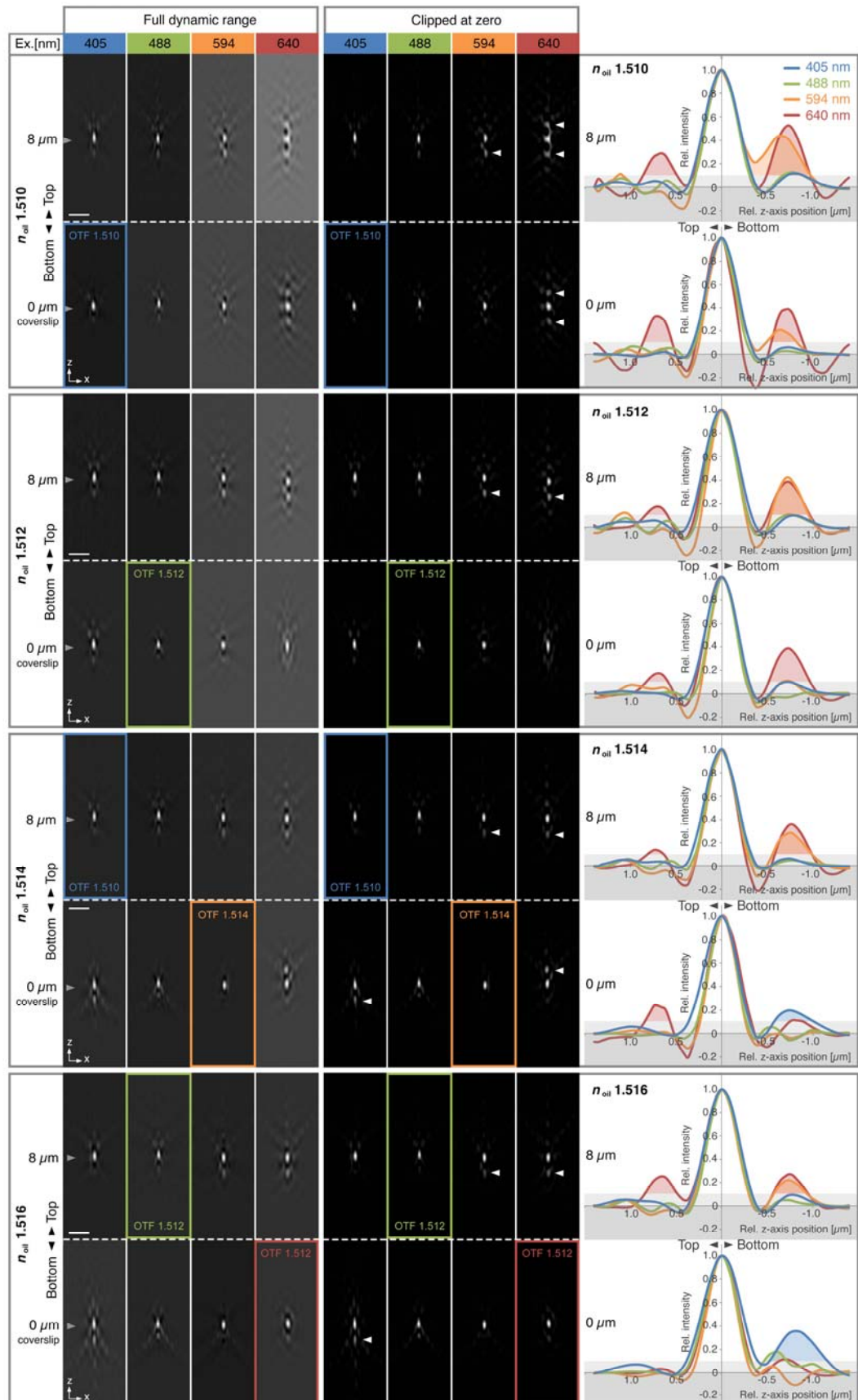
(**a**) Schematic diagram indicating the top (A), central (B), bottom (C), and full (D) sub-sections used for the reconstruction. Coverslip is on the bottom. (**b**) Orthogonal views of the resulting reconstructions. Note the artifactual patterns generated in (A) and (C) sections. Tick marks in each indicate positions of images shown in the next panel. (**c**) Representative slices of each reconstruction, corresponding to the z positions marked in (**b**). Letters represent the corresponding sub-section of the entire nucleus as shown in (**a**), while numbers represent the corresponding z-position shown in (**b**). Arrowheads denote z-wrapping artifacts, or ghost signals from other z-slices in the reconstructed segment that occur on the opposite end of a z stack to where the stack has finished acquisition on a prominent structural feature. These include shadowing and moderate 'honeycomb' patterning (inset). Scale bars: 10 μm and 2 μm (inset). Images were acquired on a GE OMX V3 Blaze instrument equipped with an Olympus 60x/1.42 PlanApo N objective and PCO edge 4.2 sCMOS cameras.



Supplementary Figure 5

Strategic considerations for imaging method selection and trade-off finding

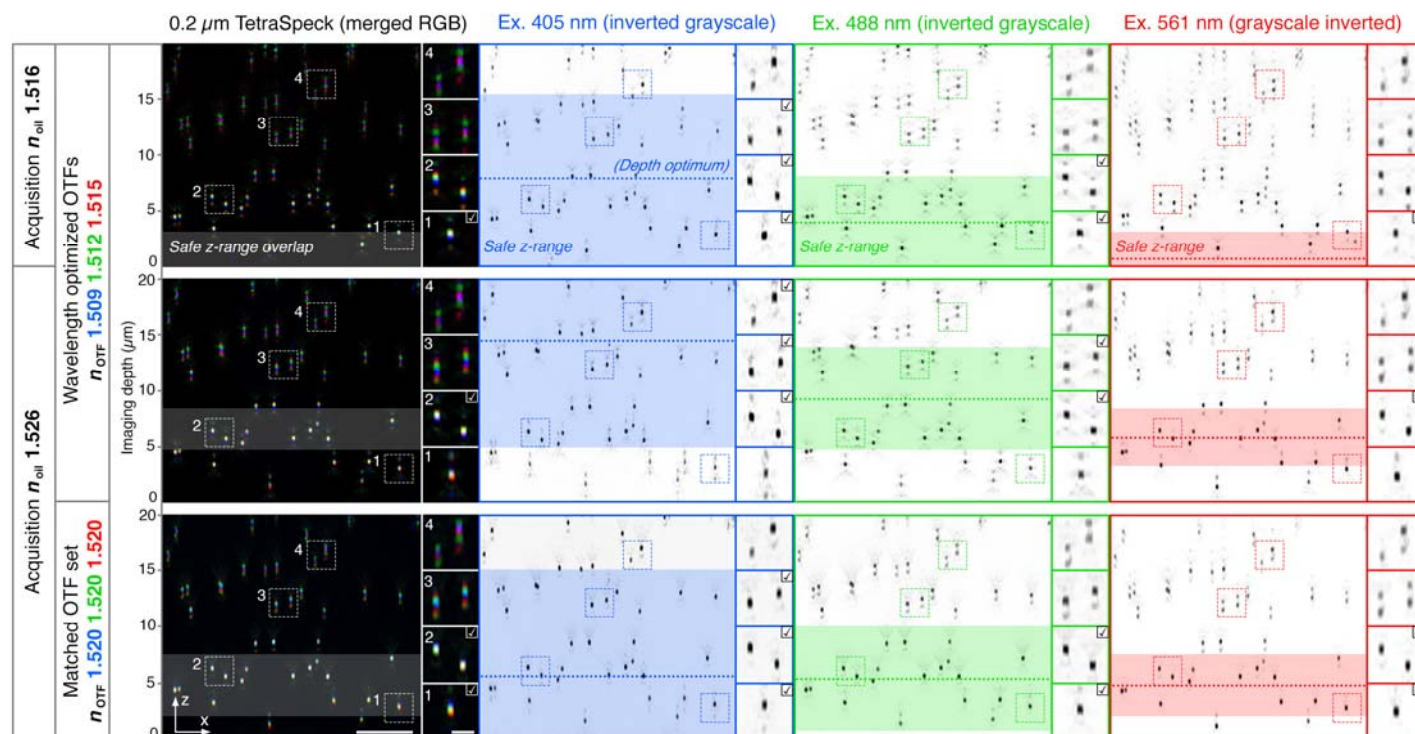
(a) Schematic diagram illustrating factors influencing the strategic decision of imaging modality selection and governed by the research question to be addressed. Also illustrated are the contributions of experimental factors affecting the relative balance between contrast and photon budget, and where these feed into technical considerations to optimize resolution, context, speed, and sample preservation. Note that improving one area will necessarily lead to trade-offs in others. (b) Schematic representation of potential factors increasing the signal and reducing unspecific background to increase the overall image contrast, which is balanced with photodamage and fluorophore bleaching not exceeding some critical threshold. Too much bleaching reduces SNR and thus the (modulation) contrast in the raw data, and will induce artifacts if the ratio is weighted too heavily towards generating high signal at the start of the dataset acquisition. The level of bleaching allowed depends on the acquisition order and may be case-dependent; however, from experience rates of up to 50% seem acceptable in most cases. The 'Channel Intensity Plot' function in SIMcheck¹³ offers a useful tool for quantifying acquisition bleaching and intensity variations affecting SNR and modulation contrast in SIM raw data.



Supplementary Figure 6

Illustration of ‘ghosting’ effect in PSFs dependent on immersion oil refractive index, wavelength, and imaging depth

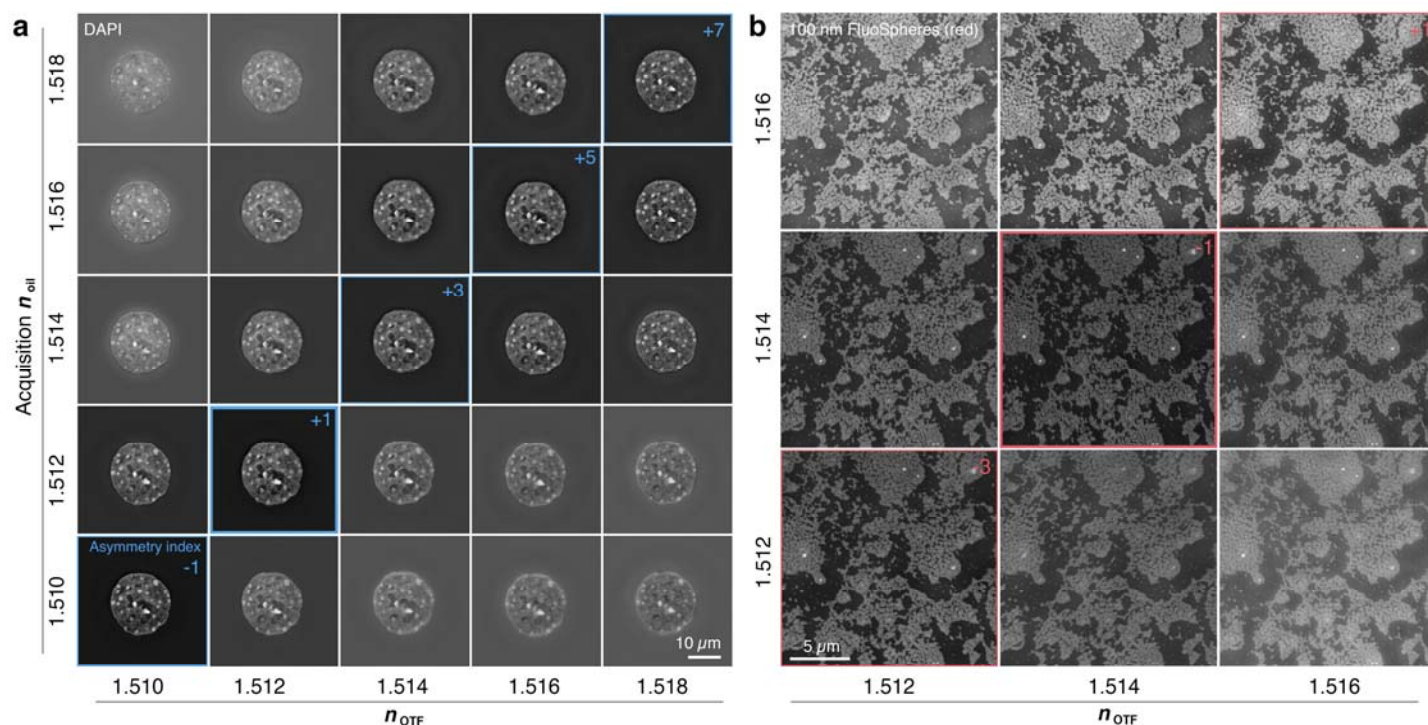
3D-SIM images of sub-diffraction PSF beads in indicated wavelengths were collected at either coverslip level (bottom, 0 μm) or the top (8 μm) of slides prepared as described, and intensity measurements averaged from 10 separate beads are plotted on the right with intensity on the y-axis and relative z-position from the center on the x-axis. The leftmost set of bead images are displayed with full bit-depth after reconstruction for clarity of artifacts, and the right set are displayed after cutting off intensities at 0 to represent images most likely seen by the user. Arrowheads indicate ‘ghost’ signals that are likely to be interpreted as ‘false-positive’ in a real sample situation. Each set of beads was imaged in a different immersion oil RI indicated on the left and above each graph and reconstructed with color-specific ‘near-optimal’ OTFs, i.e. from PSFs acquired with RIs of 1.510 (blue), 1.512 (green), 1.514 (red), 1.516 (far-red). The relative size of the lobes in the intensity graph correspond to the prominence of the spherical aberration artifacts seen in the raw images, and are dependent both on wavelength and immersion RI. Low RI’s generate more artifacts in the longer red wavelength while the reverse is true for blue wavelengths. The optimal matching of imaging conditions and OTF for each wavelength is indicated by the colored outline around certain bead images. Bars: 1 μm . Images were acquired on a GE OMX V3 Blaze instrument equipped with an Olympus 60x/1.42 PlanApo N objective and PCO edge 4.2 sCMOS cameras.



Supplementary Figure 7

SIM acquisition of 3D bead samples highlighting variations in the ‘safe z-range’ and color channel matching under different imaging conditions

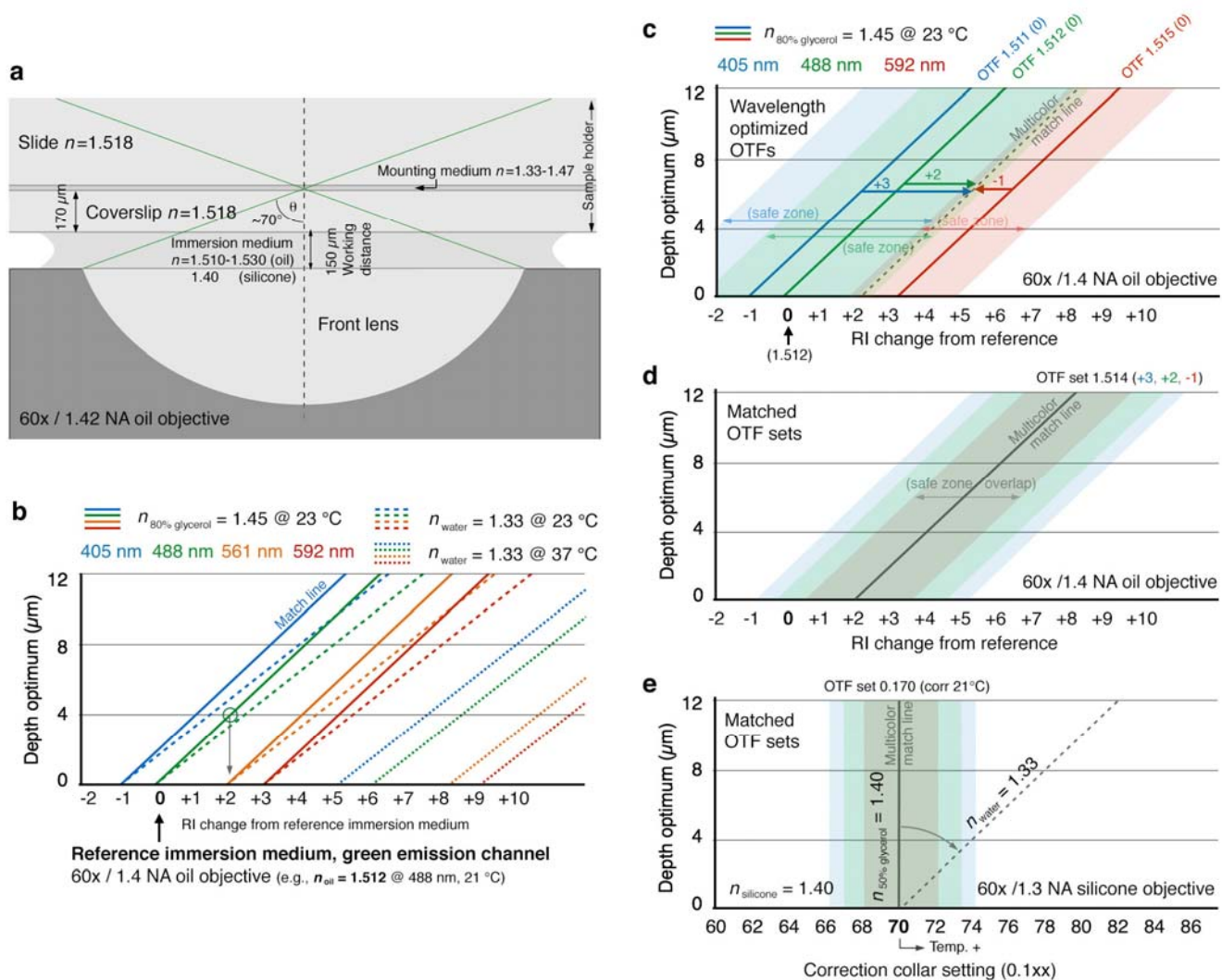
Comparisons of multicolour gel-embedded 0.2 μm TetraSpeck beads acquired using varying RI immersion oils (indicated on left) and reconstructed using different combinations of OTFs (coloured legends, also on left). The left image column shows xz-views (maximum projection) of superimposed channels (after image registration). The other columns show individual blue, green and red emission channels of the same xz-projections. In all images the coverslip is at the bottom and the y-axis shows ascending z-distance deeper into the gel. Insets show higher magnification views of individual beads with accompanying spherical aberration artifacts as a function of distance from the coverslip. Note the significant doubling/tripling of bead images in the xz-axis, especially when using an oil of too low RI (1.516) for this sample (top row). Superimposed images also reveal colour dispersion in the aberrated regions, particularly after reconstruction using channel-optimised OTFs (middle image row), rather than matched OTF sets (bottom row). Ghosting effects are most extensive in the red channel and least problematic in the blue channel. Dotted lines mark the depth optimum, colored areas around indicate the corresponding safe z-range for each channel, i.e. the range of depths within which ghosting effects are minimal. The extent and z-position of the safe z-range varies with acquisition RI, wavelength, and the OTFs used for reconstruction. Details on assembling gel-embedded bead samples are available in the **Supplementary Method**. Scale bars: 5 μm and 0.5 μm (inset). Images were acquired on a GE OMX V4 Blaze instrument equipped with an Olympus 100x/1.40 SApo objective and Photometrics Evolve EMCCD cameras.



Supplementary Figure 8

Matching of refractive indices of immersion oils used for sample acquisition and OTF measurements can compensate for PSF asymmetry

(a) Matrix of acquisitions of the same DAPI-stained C127 nucleus with varying immersion oil RIs (y-axis) reconstructed with OTFs generated from matching or varying immersion oil RIs (n_{OTF} , x-axis). Images are shown with full bit depth and no discarding of negatives to emphasize the dynamic range of the reconstruction. The immersion oil RI generating the most symmetrical PSF on the system used is 1.511, therefore the 'asymmetry index' is calculated as deviations from that metric based on the immersion RI used. This clearly shows that matching the immersion oil RI during acquisition of both the OTF and the raw image results in higher contrast and a better reconstruction than using an OTF generated with the ideal RI to reconstruct and image collected with a different immersion oil RI. (b) Example of 100 nm red bead layer showing a similar effect. The extent of mismatch compensation, however, is affected by wavelength, as PSFs of longer wavelengths are more easily distorted than shorter wavelengths (prominence of side lobes, see **Supplementary Fig. 6**). Thus, matching refractive indices n_{oil} and n_{OTF} results in a smaller window of acceptable compensation. Scale bars: 10 μm (a), 5 μm (b). Images in (a) were acquired on a GE OMX V3 instrument equipped with an Olympus 100x/1.4 PlanApo objective and Cascade II:512 EMCCD cameras, and images in (b) were acquired on a GE OMX V3 Blaze instrument equipped with an Olympus 60x/1.42 PlanApo N objective and PCO edge 4.2 sCMOS cameras.

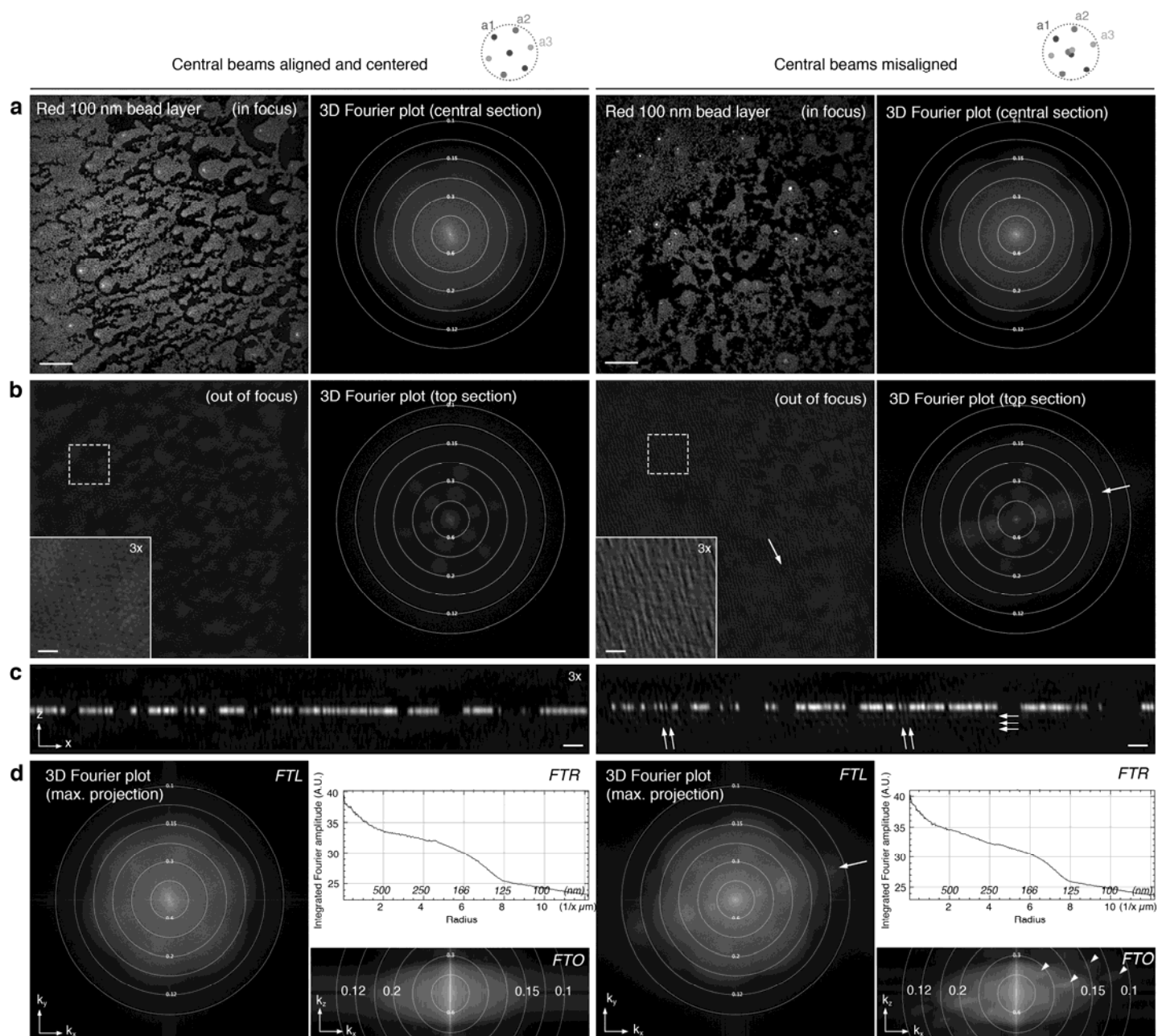


Supplementary Figure 9

Schematic representation of matching spherical aberrations of OTF and sample for multi-channel SIM imaging

(a) Representation to scale of the light path through sample components. For a high NA oil objective, the opening angle is approx. 70° . Fixed and variable refractive indices n of the different components are indicated. (b) Representation of determining optimal OTF sets based on sample depth (based on empirical data acquired on an OMX V3 Blaze system). The y-axis represents depth, or the distance of the sample region from the coverslip, in μm . The x-axis indicates the relative change in refractive index (RI) of the immersion oil from a pre-determined, system-specific reference – generally the RI of oil that gives a symmetrical PSF in the green channel at the coverslip. The optimal OTF for the 488 nm excitation channel on this system was determined (by observed symmetry of the PSF) to be at an immersion RI of 1.512 (defined as the zero point on the x-axis, as the reference value may deviate on other systems). These measurements are valid for samples mounted in glycerol with a RI of 1.47 at 23°C , with solid lines indicating the depth at which a given immersion RI will produce a symmetrical PSF in glycerol, and would thus best match to an OTF measured at the coverslip. E.g. following the green match line for 488 nm excitation, for best matching in $4 \mu\text{m}$ depth the RI

should be increased by +0.002 relative to the reference (circle, grey arrow); in this particular case an oil with RI of 1.514 should be used. Dashed lines represent the equivalent values for water-based immersion media (such as OptiMEM) at 23 °C, and dotted lines represent equivalent values for water-based immersion media at 37 °C. Note that the higher refractive index between immersion and mounting medium causes a stronger tilt along the y-axis, while a temperature increase effectively changes viscosity and thus the RI of the immersion oil, leading to a deviation from the nominal RI typically indicated for 23 °C, and shifts along the x-axis. **(c, d)** Representations of the match lines and the corresponding safe z-ranges of good reconstruction quality when using color optimized OTFs **(c)** as compared to using a set of channel specific OTFs acquired with the same RI (in this example 1.514) shifting the optimum towards the red channel **(d)**. Note that in the latter case the match lines for all channels co-align and the corresponding safe zones display a much wider overlap region. **(e)** Representation of the ideal case of having no RI mismatch achieved when combining silicone oil immersion objective and a RI matched mounting medium (e.g. 50% glycerol), and both matching the RI of the biological specimen. Theoretically this would allow aberration-free imaging throughout the working distance of the objective. In praxis, however, light scattering and specimen-inherent RI variations will become limiting, especially when the light must penetrate through many layers of biological tissue, for which correction requires more advanced adaptive optics.



Supplementary Figure 10

Evaluation of Z-stack images and corresponding 3D Fourier plots reveal inappropriate SIM beam alignment

Assessment of central (**a**) and peripheral (**b**) z-slices of reconstructed bead layer image stacks, that were acquired under otherwise ideal conditions (i.e., bright and photostable sample, minimal RI mismatch, well-matched OTF, etc.). (**a**) The central section of the corresponding 3D Fourier plots (function provided with SIMcheck 1.1) show an even frequency distribution with no obvious abnormalities or loss in resolution (top row) whether the central illumination beams (0^{th} order) of all three angles are aligned (left) or misaligned (right). However, assessing the reconstruction of out-of-focus z-planes (**b**) displays an angle-specific hatched noise pattern in the acquisition of the misaligned system (right, inset). Hatching in z-direction can also be observed in

the magnified orthogonal view (**c**, right panel), and by accompanying angle specific amplitude peaks in the peripheral region of the 3D Fourier plot (arrows). Scale bars: 5 μm and 0.5 μm (insets). (**d**) Spatial frequency components can also be viewed and evaluated via maximum projection of the 3D Fourier plots to reveal issues with SIM beam alignment. Here both lateral and orthogonal view show additional interferences as 'dots' in frequency space (arrowheads, right panel), highlighting that despite overall resolution being comparable to an aligned instrument (left), the misaligned instrument (right) is generating suboptimal SIM images. Images were acquired on a GE OMX V3 Blaze instrument equipped with an Olympus 60x/1.42 PlanApo N objective and PCO edge 4.2 sCMOS cameras.

SUPPLEMENTARY INFORMATION

Strategic and practical guidelines for successful structured illumination microscopy

Justin Demmerle^{1,8}, Cassandravictoria Innocent^{1,8}, Alison J. North², Graeme Ball^{1,3}, Marcel Müller⁴, Ezequiel Miron¹, Atsushi Matsuda^{5,6}, Ian M. Dobbie¹, Yolanda Markaki⁷, Lothar Schermelleh¹

¹Micron Advanced Bioimaging Unit, Department of Biochemistry, University of Oxford, Oxford OX1 3QU, UK

²Bio-Imaging Resource Center, The Rockefeller University, New York, NY 10065, USA.

³Current Address: Dundee Imaging Facility, School of Life Sciences, University of Dundee, Dundee, DD1 5EH, UK.

⁴Biomolecular Photonics Group, Faculty of Physics, Bielefeld University, Universitaetsstrasse 25, 33615 Bielefeld, Germany.

⁵Advanced ICT Research Institute Kobe, National Institute of Information and Communications Technology, Kobe 651-2492, Japan

⁶Graduate School of Frontier Biosciences, Osaka University, Osaka 565-0871, Japan

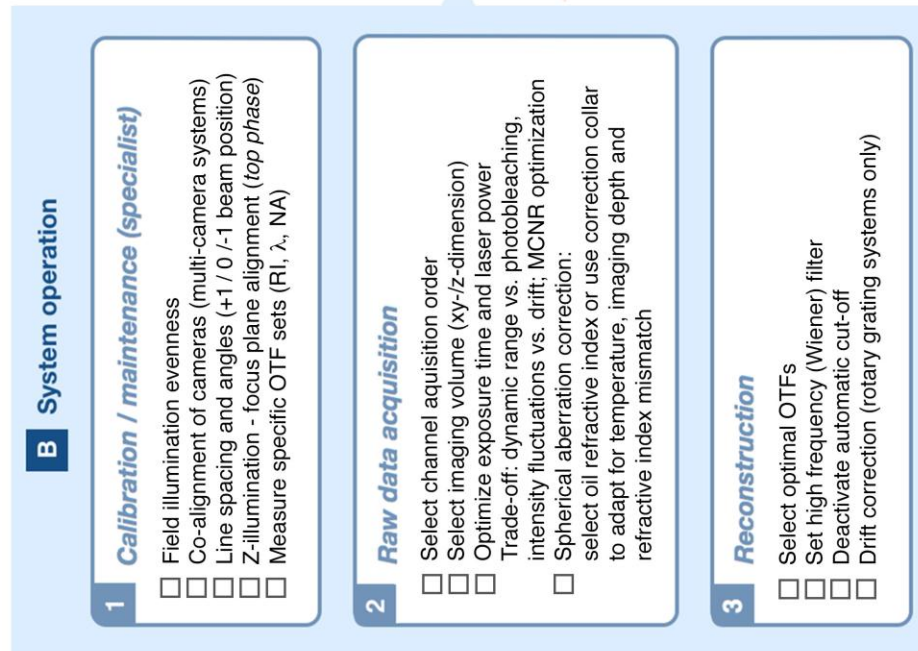
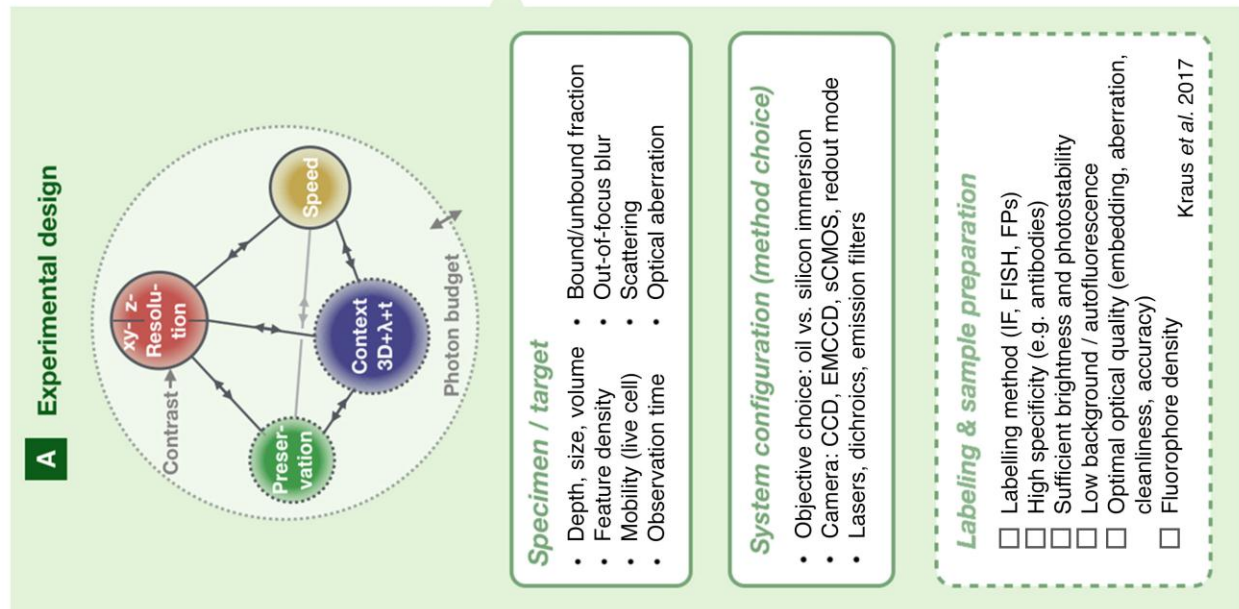
⁷David Geffen School of Medicine, Department of Biological Chemistry, UCLA, Los Angeles, CA 90095, USA

⁸These authors contributed equally to this work.

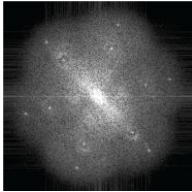
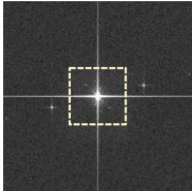
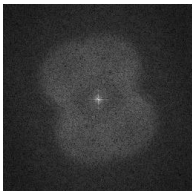
Correspondence should be addressed to L.S. (lothar.schermelleh@bioch.ox.ac.uk).

Supplementary Manual
Supplementary Table 1
Supplementary Method
Supplementary Figures 1-10

Supplementary Manual (next page) | Checklist of specific steps for ensuring high-quality SIM results. **(a)** Experimental design considerations upstream of the imaging process. **(b)** Series of checks for the user or specialist to confirm before, during, and after data acquisition. **(c)** Functionalities in the SIMcheck plugin that can help diagnose the issues raised in the left column. **(d)** Post- processing steps down-stream of the imaging procedure for completeness. All or most boxes should be checked (meaning that the issue has been considered and a solution with rationale has been reached) before making substantial conclusions from SIM data.



Supplementary Table 1 | Advanced artifact diagnostics for bespoke system setups

Artifact type	Possible cause	SIMcheck readout	Troubleshooting
<p>FFT extra dots in diagonals</p> 	<p>Deviation from $2\pi/5$ phase shift at the image level. The failure in information separation of individual orders mixes up strong center bands in higher order</p>	<p>'Reconstructed Fourier Plot'</p> <p>Dots on the diagonals.</p> <p>[System calibration] 'Illumination Phase Steps'</p> <p>Measures the phase values of the bright spot at the 1st order after FFT of the raw images, can be used to check the phase steps are really $2\pi/5$ (assuming 5 phases per angle).</p>	<p>[System]</p> <p>Check stabilities of</p> <ul style="list-style-type: none">• the illumination intensity (including the fiber shaker in OMX v2-3)• the sample/stage (including pressure of the vibration isolation table)• temperature of cameras. <p>If the step sizes of the phases still differ from $2\pi/5$, change voltages of piezo or galvo mirrors (requires service engineer).</p>
<p>FFT reproducible dots</p> 	<p>Extra beams due to unwanted reflection (stray light) in the optical path.</p>	<p>'Raw Fourier Projection'</p> <p>Reproducible spurious dots outside 1st and 2nd order stripe spots.</p>	<p>[System] Check for extra beams: remove objective, reduce illumination power to < 10%, open the shutter and project beams on a white surface on the ceiling.</p> <p>(Caution: only to be performed by a trained specialist. Do not look directly at laser light!) Optical alignment or installing apertures help to minimize it (requires service engineer).</p>
<p>FFT uneven amplitude among angles</p> 	<p>[System] Beam centering. Alternatively polarization is disrupted in a particular angle due to dichroic mirror or inaccurate K0 values.</p> <p>[Sample] Unequal refractive index or strong bleaching</p>	<p>'Raw Fourier Projection'</p> <p>Frequencies of 1 or 2 angles extend less far out.</p> <p>Angle intensity variations of <30% are still acceptable.</p>	<p>[System] To check polarization, remove objective lens, reduce illumination power to < 1% and insert a polarizer to examine if the illumination intensity goes down as the polarizer is rotated. This problem is angle- and possibly wavelength-dependent. Exchange the dichroic mirror.</p> <p>[Sample] Check bleaching rate.</p>

ADDITIONAL SUPPLEMENTARY MATERIALS

REAGENTS

- TetraSpeck Fluorescent Microspheres 0.2 μm diameter (ThermoFisher, cat. no. T7280)
- Phytigel powder (Sigma, cat. no. P8169-100G)
- CyGEL (BioStatus, cat. no. CY10500)
- Silicon gasket (Harvard Apparatus)
- Dulbecco's PBS (Sigma, cat. no. D8537)
- Calcium Chloride CaCl_2 (Sigma, cat. no. 10043-52-4)
- Borosilicate precision cover glasses, thickness No. 1.5H ($170 \pm 5 \mu\text{m}$); 18x18 mm or 22x22 mm (e.g., Marienfeld Superior, cat. no. 0107032)
- Quick-drying nail polish, preferably bright colored metallic, or CoverGrip coverslip sealant (Biotium, cat. no. 23005)

REAGENT SETUP

- CyGEL is liquid when stored on ice and transitions to a gel at approx. 23 °C. PBS-primed CyGEL was prepared by adding 12.8 μl of the supplied 40x PBS to a pre-cooled vial of CyGEL on ice. A pre-cooled pipette tip was used when mixing beads with the CyGEL to keep it in the liquid state until ready.
- Phytigel was prepared by adding 0.25 g of Phytigel powder (Sigma, P8169-100G) to 50 ml of rapidly stirring PBS (plus CaCl_2). Microwaving (or autoclaving) the solution to 80-90 °C was required in order to fully dissolve the powder. The gel was cooled to 40-50 °C before adding the beads, then mixed with the beads before it solidified at around 32 °C.

NOTE

- Bead suspensions were prepared in either CyGEL (BioStatus) or Phytigel (Sigma). The refractive index of CyGEL is reported by BioStatus to be 1.37 and the measured refractive index of this Phytigel preparation was 1.338.

1| Well slides for 3D bead samples are prepared by applying an 18 mm square section of a 100 μm thick silicon gasket (Harvard Apparatus) to a pre-cleaned glass slide. A hole approximately 3 mm square is cut out of the gasket using a razor blade, to form a small well.

2| Rapidly suspend 4 μl of 0.2 μm diameter TetraSpeck beads in 100 μl of cold CyGEL or warm Phytigel. Immediately pipette approx. 50 μl into the gasket well.

▲ CRITICAL STEP 0.1 μm beads may be more stringent for assessing spherical aberration, but the blue signal is easier to detect using 0.2 μm beads, therefore these were used for assessing chromatic shift.

3| Press a pre-cleaned high performance coverslip (18 mm square) firmly on top to extrude excess gel solution before it solidifies, to ensure the coverslip lays flat on the gasket.

4| Seal around the edges of the coverslip with quick-dry nail polish.

▲ CRITICAL STEP Gel slides should be stored at room temperature and used within 1-2 d of preparation to ensure that the gel does not dry out.